Engineering Structures 155 (2018) 394–409

Contents lists available at ScienceDirect

Engineering Structures

journal homepage: www.elsevier.com/locate/engstruct

Effects of vertical stresses and flanges on seismic behavior of unreinforced brick masonry

Hizb Ullah Sajid*, Mohammad Ashraf, Qaisar Ali, Sikandar Hayat Sajid

Department of Civil Engineering, University of Engineering and Technology, Peshawar, Pakistan

ARTICLE INFO

Keywords:
Brick masonry
Vertical stresses
Flange effects
In-plane response
Seismic behavior

ABSTRACT

Lateral in-plane response plays crucial role in seismic behavior of masonry structures. The aim of this article is to experimentally investigate the effects of vertical stresses and flanges (transverse walls) on the lateral in-plane response of the unreinforced brick masonry (URBM) walls. The experimental work included lateral in-plane quasi-static cyclic tests on full-scale walls (both with & without flanges). The vertical stresses resulting from typical single and two story unreinforced masonry buildings were simulated on full scale URBM walls. Flanges were introduced at both ends of the in-plane wall in single direction. In essence, the lateral in-plane stiffness & strength, deformability and energy dissipation of the two classes of walls are compared and the differences are quantified to help understand the effects of flanges on the in-plane response of masonry walls. The resulting damage mechanism and failure modes for each case are critically analyzed. The experimental results indicate that both vertical stresses and flanges incorporation significantly improved seismic response of URBM walls. In addition, the participation of flanges is critical in both vertical stress conditions.

1. Introduction

Brick masonry is one of the most widely used building material in construction industry throughout the world. For centuries, masonry construction has been preferred primarily due to plentiful and inexpensive availability of constituent materials and ease of construction. Historically, such type of construction is located in areas that are prone to seismic activity [1]. URBM offers a weak response when subjected to lateral loads such as earthquake. As witnessed in 2005 Kashmir, Pakistan earthquake, and November 2015 earthquake in Afghanistan and Pakistan, URBM suffered heavy damages [2–8]. Masonry structures (brick and stone) suffered yet again in the more recent earthquakes of 2009 and 2016 in Italy [9–12] and 2015 in Nepal [13,14]. These events have further strengthened the need of continuing research to understand and improve unreinforced masonry construction. It is evident, that such type of construction, although more economical and popular, pose high risk to the safety of masses during earthquakes. Extensive research has been carried out and more work is in progress to understand the behavior of masonry structures and to develop better design guidelines for the same.

Seismic capacity of masonry structure is affected by a variety of parameters that include aspect ratio, level of vertical stress, mechanical properties of masonry and its constituents and flanges This paper investigates the effects of vertical stresses and boundary conditions (flanges) on the in-plane behavior of the URBM structures.

Vertical stresses are inherently present in all load-bearing URBM structures. Vertical stresses resulting from the diaphragm, adjacent parts of the buildings and occupancy loads, constitute one of the important parameter which influence the behavior of URBM under the action of lateral loads. A number of researchers have studied vertical stresses for their effects on masonry behavior and response. Research work carried out by (Magenes, G., Calvi [15], Irimies & Bia [16]; Yi et al. [17]; Haach et al. [18]; Tomaževič & Weiss [19]; Salmanpour et al. [20]; Salmanpour et al. [21], Salmanpour et al. [22]; Javed et al. [23]) utilized both solid and hollow brick and block masonry to study the effects of vertical stresses. Quasi-static cyclic testing has been performed in most of these studies due to its advantages over other types of testing techniques [24].

Most of these researchers tested isolated masonry piers or walls either full scale or half scaled. However, Irimies & Bia [16] also incorporated flanges in the specimens. Axial loads, masonry unit types, geometrical characteristics and material strengths were varied to study their effects on response parameters. All the researchers concluded that vertical stress is a principal parameter that affects the strength and deformability characteristics of the masonry.

Apart from vertical stresses, boundary conditions, particularly flanges, also play important role in the load in the behavior of URBM. Boundary conditions though inherently present in the brick masonry

* Corresponding author.
E-mail addresses: hezb_uetian@yahoo.com (H.U. Sajid), engineerashraf@yahoo.com (M. Ashraf), drqaisarali@uetpeshawar.edu.pk (Q. Ali), shsajid1@gmail.com (S.H. Sajid).

https://doi.org/10.1016/j.engstruct.2017.11.013
Received 21 April 2017; Received in revised form 3 October 2017; Accepted 8 November 2017
0141-0296/ © 2017 Elsevier Ltd. All rights reserved.

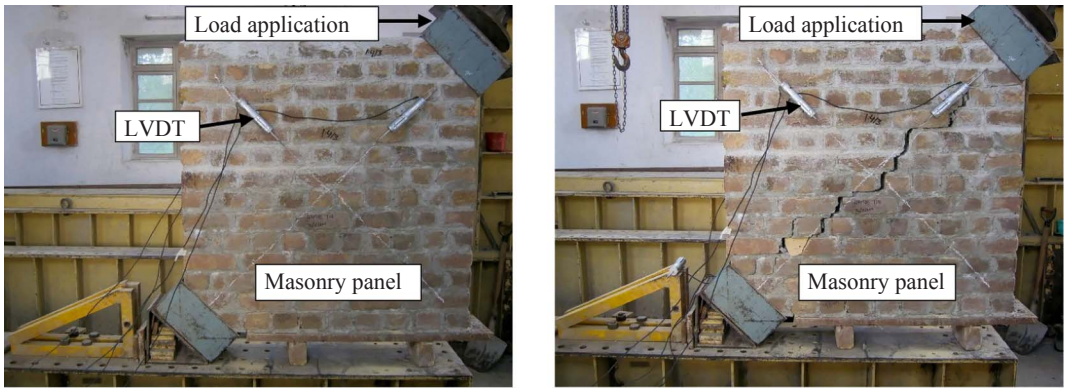

Fig. 1. Compressive strength testing of brick masonry panels.

walls, are frequently ignored in the research owing to their limited contribution. Limited research is available in literature on the contribution of flanges on the deformability and strength characteristics of URBM walls. Earliest studies on masonry carried out by Tomaževič et al. [25], Costley and Abrams [26], and Tomaževič [1] suggested the need to evaluate flanges effects on masonry response. More recent work on flanges participation was reported by Paquette and Bruneau [27], Moon [28] and Yi et al. [29].

Moon [28] carried out one of the earliest and most comprehensive work to investigate the effects of flanges on capacity and response of URBM. Moon [28] conducted lateral load tests on a two storey full scale unreinforced masonry (URM) structure before and after retrofitting. The variables of interest included overturning effects, flanges participation and global rocking. Based on the results, a number of modifications has been suggested in the current FEMA 356 model [30] for in-plane analysis of perforated walls. For the purpose of modification in the FEMA 356 [30] model, flanges have been divided into three categories which include compressions flange, global tension flange and component tension flange. The research observed considerable participation of each category of flange in influencing the capacity and failure modes in in-plane URBM walls.

Yi et al. [31] developed a new pier model to investigate the effects of flanges on the behavior and response of URM piers. The proposed model is modification of the effective pier model developed by Yi et al. [29]. The modified model is analyzed for a non-rectangular URM pier to study flange effects. Russell and Ingham [32], Russell and Ingham [33] and Russell et al. [34] studied flanges contribution for material and loading characteristics experienced in brick masonry structures in New Zealand. Their results confirmed the accuracy of the model proposed by Yi et al. [31] for estimating strength of flanged in-plane wall. Furthermore, the results emphasized the effects of flanges on failure mode and lateral strength of unreinforced masonry.

Most recent work on flanges contribution in URBM has been reported by Khanmohammadi et al. [35] who tested four half scaled masonry specimens. The research work mainly focuses on block masonry, with either solid or perforated geometric nature and made comparisons between experimental work and proposed models that yielded acceptable prediction under controlled conditions.

Due to limited work on flanged unreinforced brick masonry (FURBM), further investigation is required to yield data for developing acceptable analytical models for capacity and behavior prediction of masonry. Furthermore, due to the variability in material characteristics and different geometric as well as loading configurations that were applied by various researchers, the results obtained do not have straightforward application to the masonry structures that constitute building stock of developing countries. The research work presented in this article encompasses the effects of target variables on baked clay solid brick units that are typically employed in construction industry in developing countries.

2. Experimental program

To investigate the effects of vertical stresses and flanges on strength and deformability characteristics of URBM, a detailed experimental scheme was designed. The experimental program included selection of representative constituent materials for construction of test specimens, determination of constituent material properties, construction of full-scale specimens and quasi-static cyclic testing of specimens.

2.1. Material properties

Prior to fabrication of specimens, a preliminary study was carried out to select representative materials to be used in the specimens. All the specimens were constructed using baked clay solid bricks having nominal size of 229 × 114 × 76 mm that are commonly used in the local construction industry in Pakistan. For brick units, initial rate of absorption and compressive strength were determined according to ASTM C67-16 [36] and the cement mortar compressive strength was determined following ASTM C109 [37]. The water-cement ratio was decided based on the consistency of the mortar in order to achieve a workable mix. To characterize the compressive strength and diagonal tension behavior of masonry, masonry assemblages were prepared and tested in compliance with test protocols of ASTM C1314 [38] and ASTM E59 [39], respectively, as shown in Fig. 1. Table 1 represents mechanical properties of constituent materials.

2.2. Construciont of full scale walls

In order to investigate the effects of variables under consideration, a total of four (04) full-scale URBM specimens were constructed. The specimens were named as S1, SF1, S2 and SF2. Specimens S1 and S2 are full scale perforated walls without incorporation of flanges. Specimens SF1 and SF2 are full scale perforated walls with incorporation of flanges. The numeric values, 1 and 2, in the specimen IDs (S1, S2, SF1,

Table 1
Mechanical properties of constituent materials.

Material	Property	Results (average)	Testing Standard
Brick units	Compressive strength (MPa)	16.20	ASTM C67-3a
Brick units	Initial rate of absorption (kg/min)	0.07	ASTM C67-14
Cement mortar (1:4)	Compressive strength (MPa)	7.95	ASTM C109
Brick masonry	Compressive strength (MPa)	4.34	ASTM C1314
Brick masonry	Diagonal tensile strength (MPa)	0.17	ASTM E519

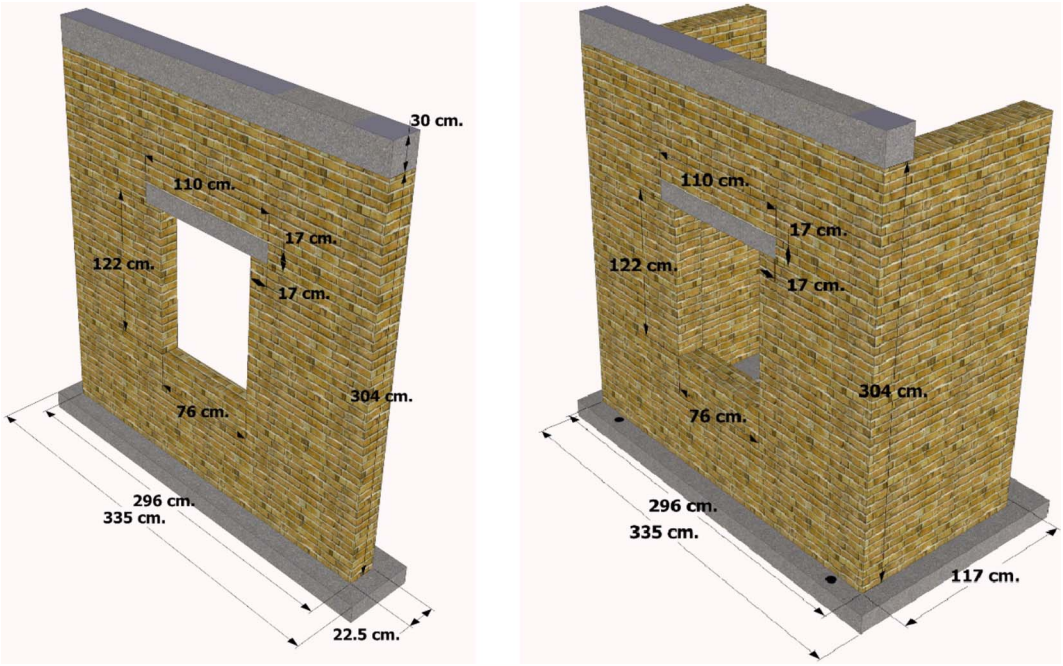

Fig. 2. Geometric detailing of specimen S1, SF1 (isolated masonry wall) and S2, SF2 (flanged masonry wall).

Fig. 3. Typical test specimen.

SF2) represent the vertical stress levels that are typically experienced in single and double storey residential room (366 cm × 457 cm), respectively. Each specimen was 296 cm long and 304 cm tall and have a thickness of 225 mm. English bond pattern was utilized in the specimens. Average thickness of mortar joints was around 1.25 cm. Typical test specimens are shown in Figs. 2 and 3. Specimen S1 and S2 are isolated walls with no flanges at the ends. Specimen SF1 and SF2 are provided with flanges along one direction at both ends. Each specimen contains two piers with identical geometric characteristics. A 17-cm thick lintel beam is provided in both specimens.

Fabrication process of full-scale URBM specimens was divided in two phases. In the first phase, reinforced concrete pad was constructed to serve as platform for the specimen. In the second phase, full-scale URBM specimens were constructed. The platform for the brick masonry specimens was constructed using 1:2:4 concrete mix. Upon this platform the test walls were then fabricated. In order to make sure that platform will be stable and remain intact during testing, the footing was anchored to the floor using anchor-bolt system, as shown in Fig. 4. Epoxy grout was used for installing anchoring system in the floor.

Lateral loading is imposed on the specimens with a reinforced concrete beam on each specimen. Vertical stresses were applied on masonry walls using dead load of steel beam and vertical load cell. Fixed-cantilever condition was simulated in both specimens. Geometric as well as loading details of test specimens are given in Table 2.

2.3. Test setup

Instrumentation plan for typical test specimens is shown in Fig. 5. Linear variable displacement transducers (LVDTs) were installed for recording displacements at various target locations to capture wall mechanism, as shown in Fig. 5. LVDT-1 was installed on the front face at the top of the wall, at horizontal level, to record the horizontal displacement of the wall. This transducer also served as control gauge. LVDT-2 and LVDT-3 were installed at top of north and south pier respectively, to record top displacement of individual piers. LVDT-4 was installed at mid point of lintel beam. The data from this transducer will be used to establish sliding of piers, if any. LVDT-5 was installed at the bottom of the window opening. LVDT-6 is provided at vertical level, at the bottom of the wall to study global rocking of the specimen. LVDT-7 is provided at horizontal level, at the bottom of the wall, to capture global sliding of the specimen. LVDT-8 and LVDT-9 were installed at the top corners of the wall, in the out-of-plane direction. The purpose of these transducers were to capture any possible out-of-plane rotation of the specimen so that test can be stopped in the event of excessive out-of-plane rotation of the specimen. LVDTs installed on the specimens were capable of recording a linear displacement of 50 mm in a single direction. For recording displacement in both negative and positive direction of loading, the LVDTs were set at 25 mm at the start of the test. Hence, they were able to measure a displacement up to 25 mm in either positive or negative direction, which was within the anticipated displacement range of test specimens. LVDTs provide a convenient mean to record linear displacement in masonry structures and have been used successfully in previous studies.

All the test specimens were tested inside the loading frame of Structural Engineering Laboratory at Department of Civil Engineering, University of Engineering and Technology, Peshawar - Pakistan. On global level, the specimens were fixed at bottom and were free to translate at the top, thereby simulating cantilever boundary condition. Piers were in double fixed condition. Vertical and horizontal loads were applied on the specimens using hydraulic jacks that were operated

Fig. 4. Geometric detailing and finished platform for test specimens.

Table 2
Geometric and loading details of test specimens.

Specimen ID		S1, SF1	S2, SF2
Wall Dimensions	L (cm)	296	296
	H (cm)	304	304
Pier Dimensions	Lp (cm)	110	110
	H_p (cm)	122	122
	t_p (cm)	22.5	22.5
	Aspect Ratio	1.11	1.11
Vertical stress at top of wall (MPa)		0.05	0.16
Vertical stress at top of pier (MPa)		0.08	0.23

using a hydraulic pump. Load cells, having capacity of 500 kN, were used to apply horizontal and vertical loads. Loading shoes were attached to both ends of the top concrete beam. This was two ensure that same loading conditions are simulated in both push and pull (positive and negative displacement) cycles. Two steel plates were placed on the top R.C. beam. Lubricated steel rollers were placed on each steel plate. A steel beam was placed on this assembly and vertical load was then applied to the steel beam. This mechanism was used to simulate the actual lateral loading conditions experienced by a full-scale masonry wall. In case of specimen SF1, the vertical load was small, hence it was applied on flanges using dead load of steel beams and sand bags. However, in case of specimen SF2, the vertical load was not manageable using dead loads, hence hydraulic jack load was used for both in-plane and out-of-plane walls. For this purpose, two short steel beams were separately designed to carry the target loads. The load from vertical load cell was transferred to the main steel beam first. The load from the steel beam was transferred to short steel beams, from where it was distributed to in-plane and out-of-plane walls. The location of short

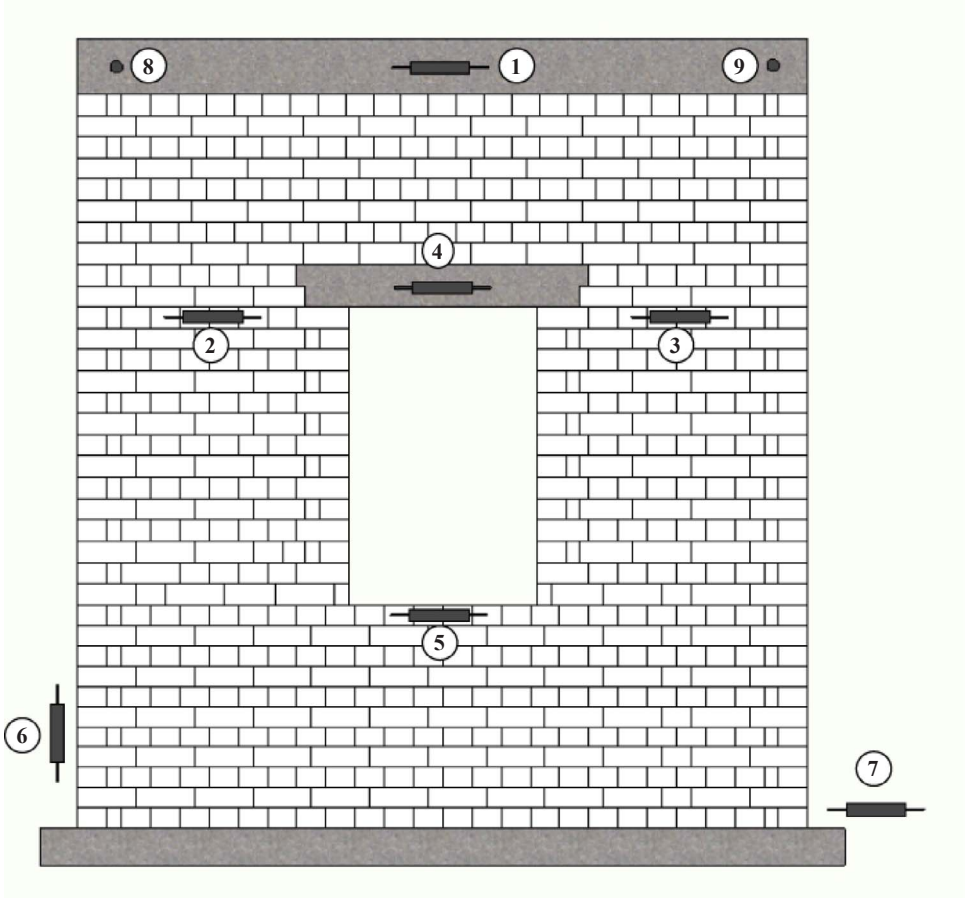

Fig. 5. Instrumentation plan of typical test specimen.

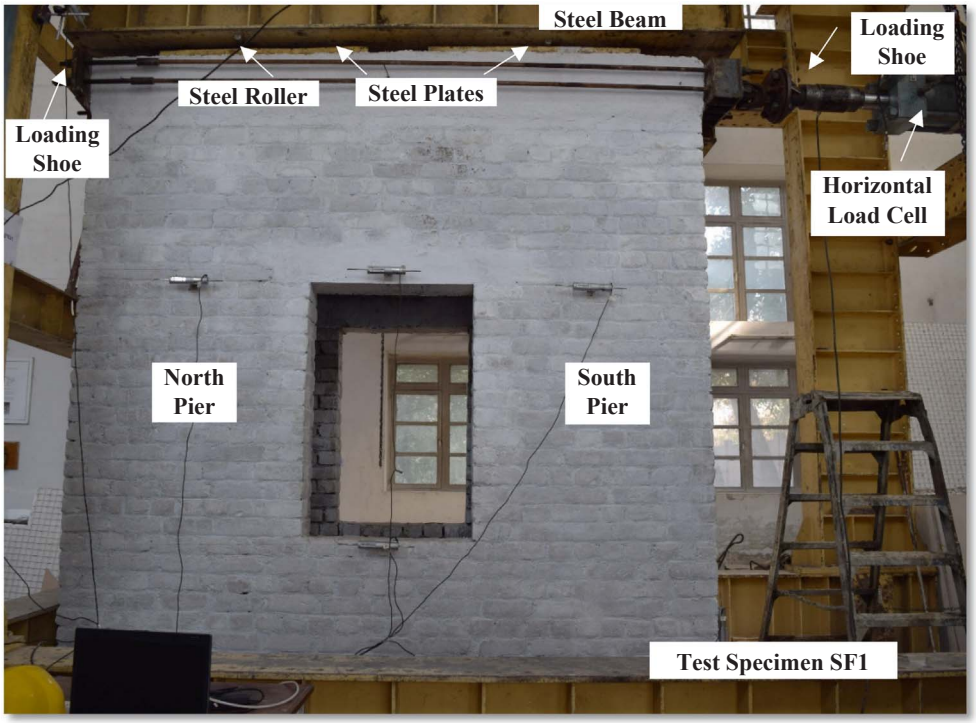

Fig. 6. Instrumentation and loading assembly of specimen SF1.

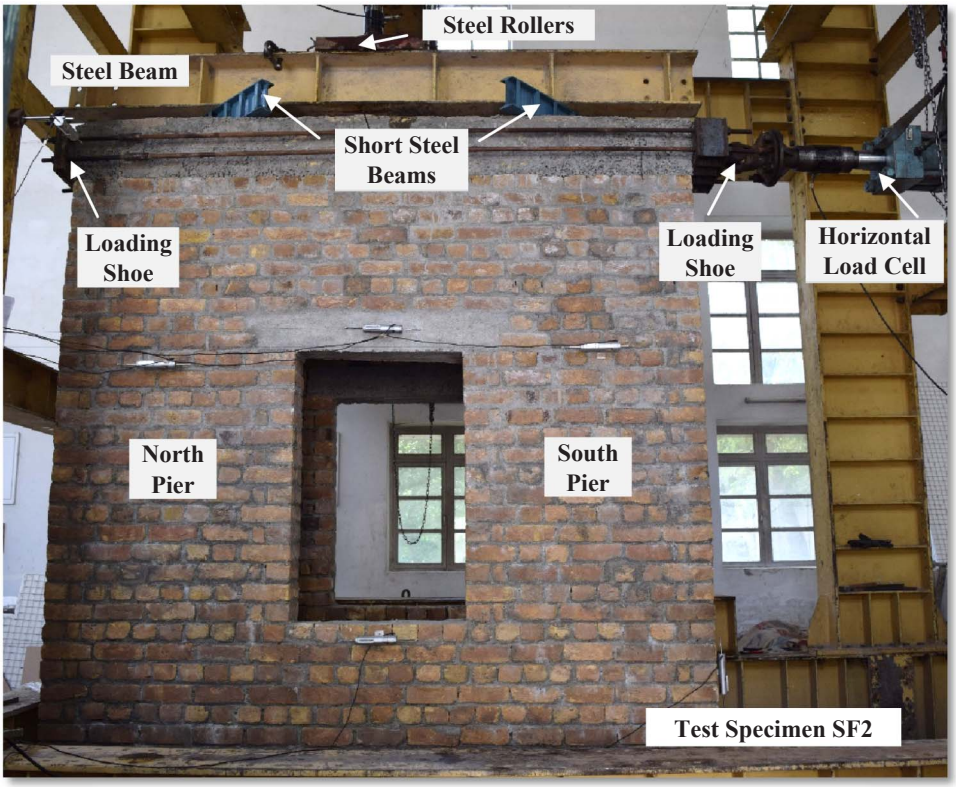

Fig. 7. Instrumentation and loading assembly of specimen SF2.

beams and long steel beam was set such that desired load levels are produced at both in-plane and out-of-plan walls. The horizontal loads were applied to in-plane walls. The testing setup and loading assembly for all the specimens is shown in Figs. 6 and 7. Fig. 8 depicts hydraulic pump system and data acquisition system used during testing of specimens.

2.4. Test procedure

Quasi-static cyclic test was carried out on each specimen to evaluate effects of target variables on response parameters. Quasi-static cyclic testing was selected herein due to its advantages over other type of dynamic testing procedures. These include the ease of applying a higher magnitude force to the test specimens and relatively inexpensive

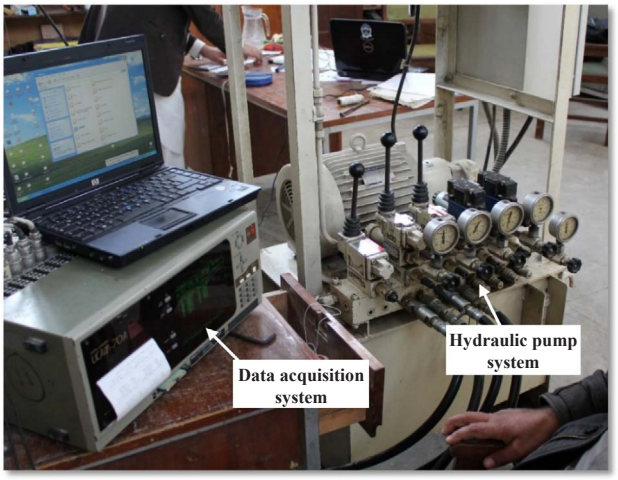

Fig. 8. Data acquisition system and hydraulic pump system.

equipment [24]. Furthermore, the progression of damage mechanism and crack patterns can be closely captured in such type of test. Owing to these advantages, researchers have frequently adopted quasi-static cyclic testing for investigating seismic behavior of unreinforced brick masonry [5,6,16,17,20,22,23,34,35,41,46]. Typical testing setup

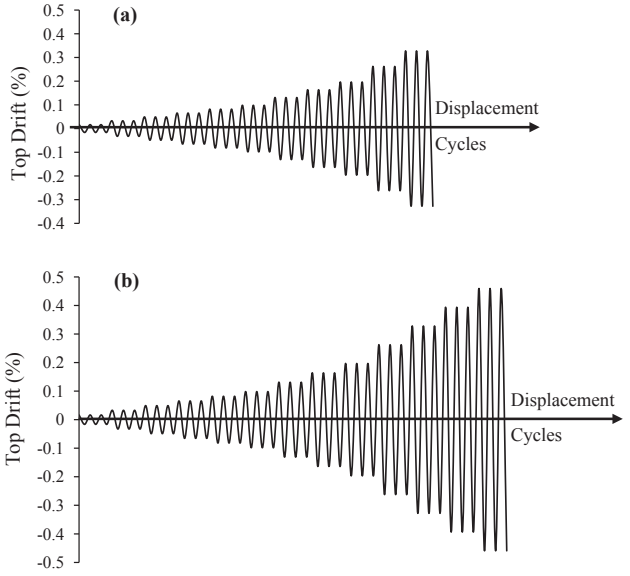

Fig. 10. Displacement time history: (a) S1 and SF1 walls, (b) S2 and SF2 walls.

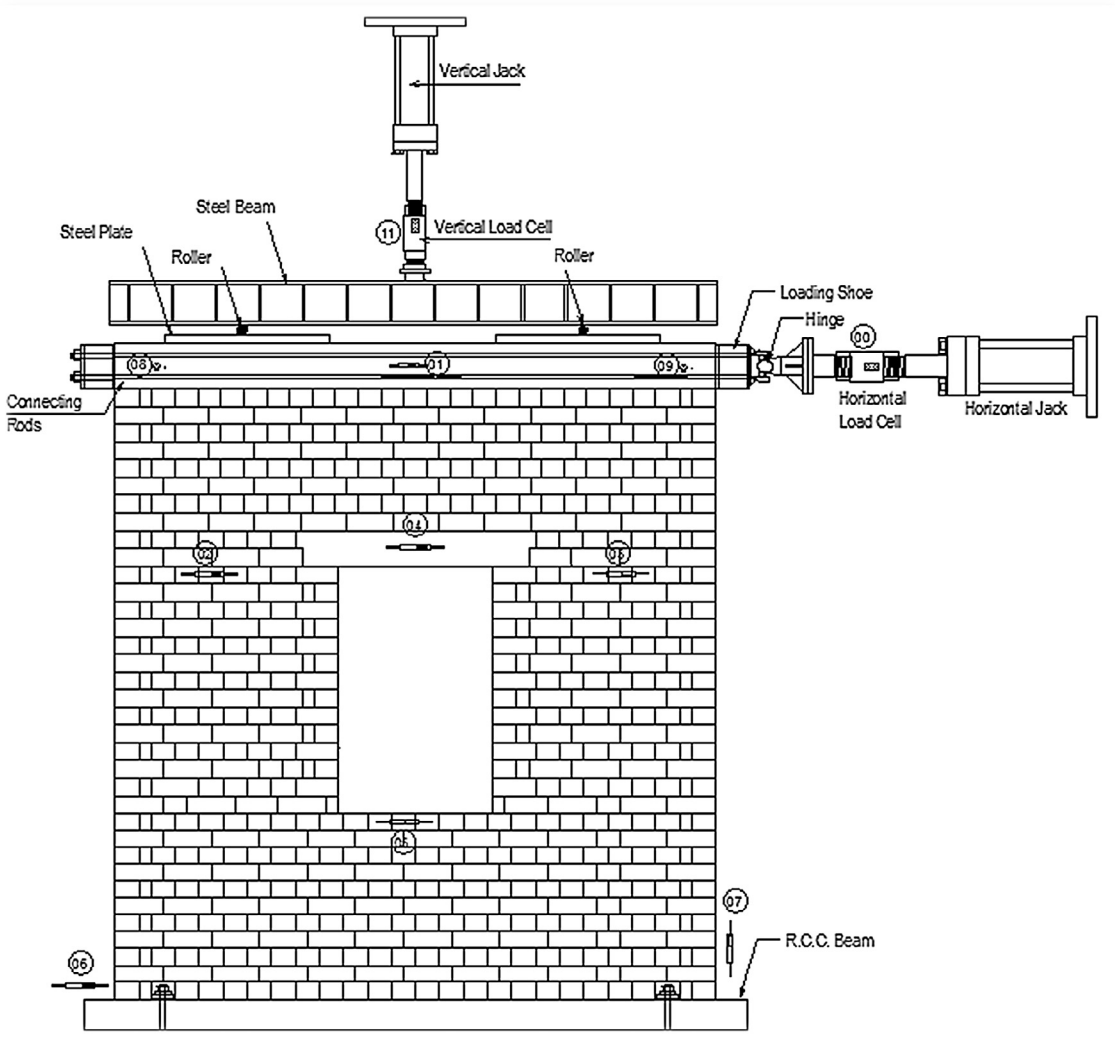

Fig. 9. Typical test setup of specimen SF1 and SF2.

shown in Fig. 9. Both force and displacement control cycles were applied with stepwise linearly increasing pattern to simulate lateral forces on the specimen. Each force or displacement cycle was repeated three times. Force and displacement as well as cracks initiation and propagation was monitored during and after completion of the specified cycles. Typical displacement histories imposed on specimens are shown in Fig. 10. Displacement loading cycles were continued until either 20 percent drop occurred in the lateral strength capacity of specimen or severe physical damage occurred in the specimen. The rates of displacement varied from an average of 50 seconds per cycle for low displacement cycles to an average of 150 seconds per cycle during high displacement

3. Test results and discussions

In this section, results of experiments carried out on each test specimen are presented. Data obtained from various gauges is processed to determine target parameters and behavior under lateral loading. Damage mechanism and failure modes, force-displacement behavior of wall and pier, and spandrel behavior for each specimen are discussed. Lateral strength, stiffness, energy dissipation, ductility and damping are calculated for each specimen. Furthermore, effects of vertical stresses and flanges on the above parameters of interest are also discussed.

3.1. Damage mechanism

Figs. 11 and 12 depict the final crack patterns of each test specimen while Figs. 13–15 represent propagations of cracks at different limit states (IO, LS and CP) in the walls as per definition of ASCE 41-06 [40] performance levels. It is worth mentioning that three cycles of each drift ratio were applied, therefore all crack patterns shown in Figs. 11 and 12 are corresponding to third cycle. All walls, except S1, exhibited similar elastic behavior up to drift of 0.045% and a load of about 16 kN. In S1 wall, a minor bed joint crack was observed at a drift of 0.035%. First cracks appeared in specimens at the corners of the window opening in the walls. In case of low vertical stress specimens (S1 and SF1), cracks initiated at window opening corners propagated diagonally towards respective top corners of the specimens. Furthermore, stepped diagonal cracks passing through mortar joints were observed at higher drift ratios. No masonry units breakage was observed except at corners. The initial diagonal cracks from window opening corner to the respective bottom and top corners of the wall were the major cracks observed in these specimens and they continued to increase in size at higher drift ratios. Other cracks were minor in nature.

In case of high vertical stress specimens (S2 and SF2), cracks initiated at vertical face of lintel beam and propagated diagonally in bottom direction at lower drift ratios and in top direction during higher drift ratios. Cracks also initiated in pier location of these walls during initial drift ratios. Diagonal cracks passed both through joints and masonry units during high displacement cycles. Petry and Beyer [41] reported similar steepness of diagonal cracks and passing of diagonal cracks through masonry units under high vertical stresses in unreinforced masonry. Furthermore, breakage of masonry units was observed at higher drift ratios. Due to high vertical stress in these specimens, shear failure dominated and hence more abrupt failure was observed which is consistent with results reported by Petry and Beyer [42].

Flanged specimens (SF1 and SF2) sustained relatively less damage, as evident from Figs. 14 and 15. Flanged portion of SF1 sustained more damaged as compared to flanged portions of SF2 wall. At 0.20% drift ratio, diagonal crack was observed in upper part of flanged portion of SF1 wall. At higher drift ratios, more diagonal cracks as well as stepped vertical crack continuing throughout height of flanged portion was observed in SF1 wall. Flanged portion of SF2 wall remained undamaged till 0.40% drift ratio. Diagonal cracks and stepped vertical cracks, both of relatively lesser extent was compared to SF1 wall, were observed at a drift ratio of 0.46%. Spandrel portions of all wall specimens remain undamaged throughout the test.

3.2. Force deformation behavior

Force-deformation behavior of each test specimen, as shown in Figs. 16 and 17, is discussed below:

3.2.1. Wall S1

Tight loops were observed till drift ratio of 0.08% which indicates low energy dissipation. Beyond 0.08% drift ratio, loops widened at high rate indicating high energy dissipation and damage in specimen. Stiffness degradation started at 0.04% drift ratio. Stiffness degradation occurred more rapidly in positive loading as compared to negative loading due to more damages in negative loading cycles. At higher drift ratios, rocking behavior dominated the specimen response as evident from end loops and damage pattern. Low vertical stresses favored flexural response which is consistent with the results reported in Petry

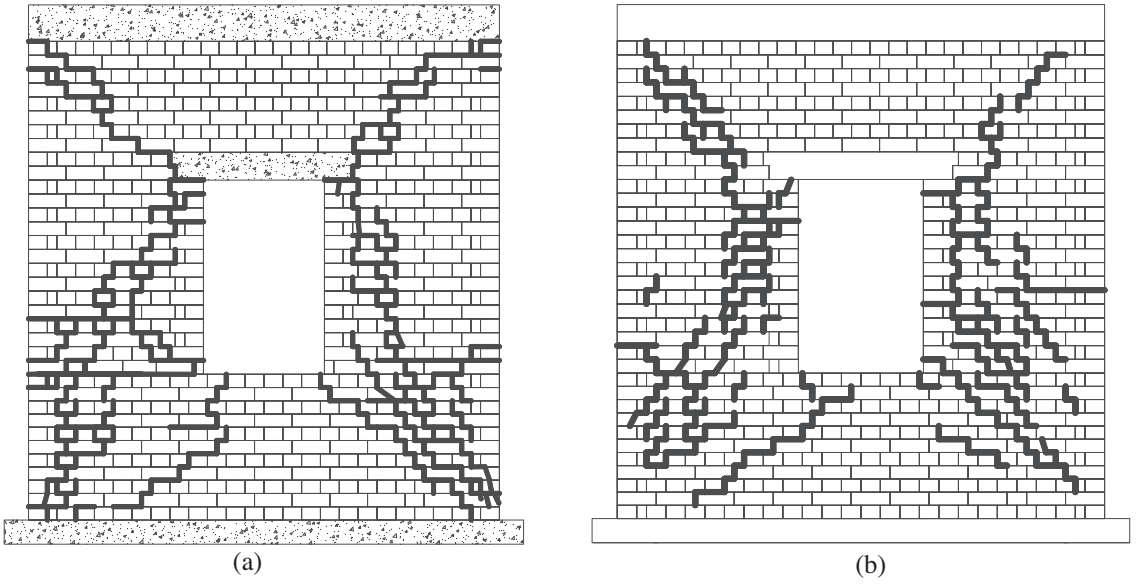

Fig. 11. Crack patterns: (a) S1 wall, (b) S2 wall.

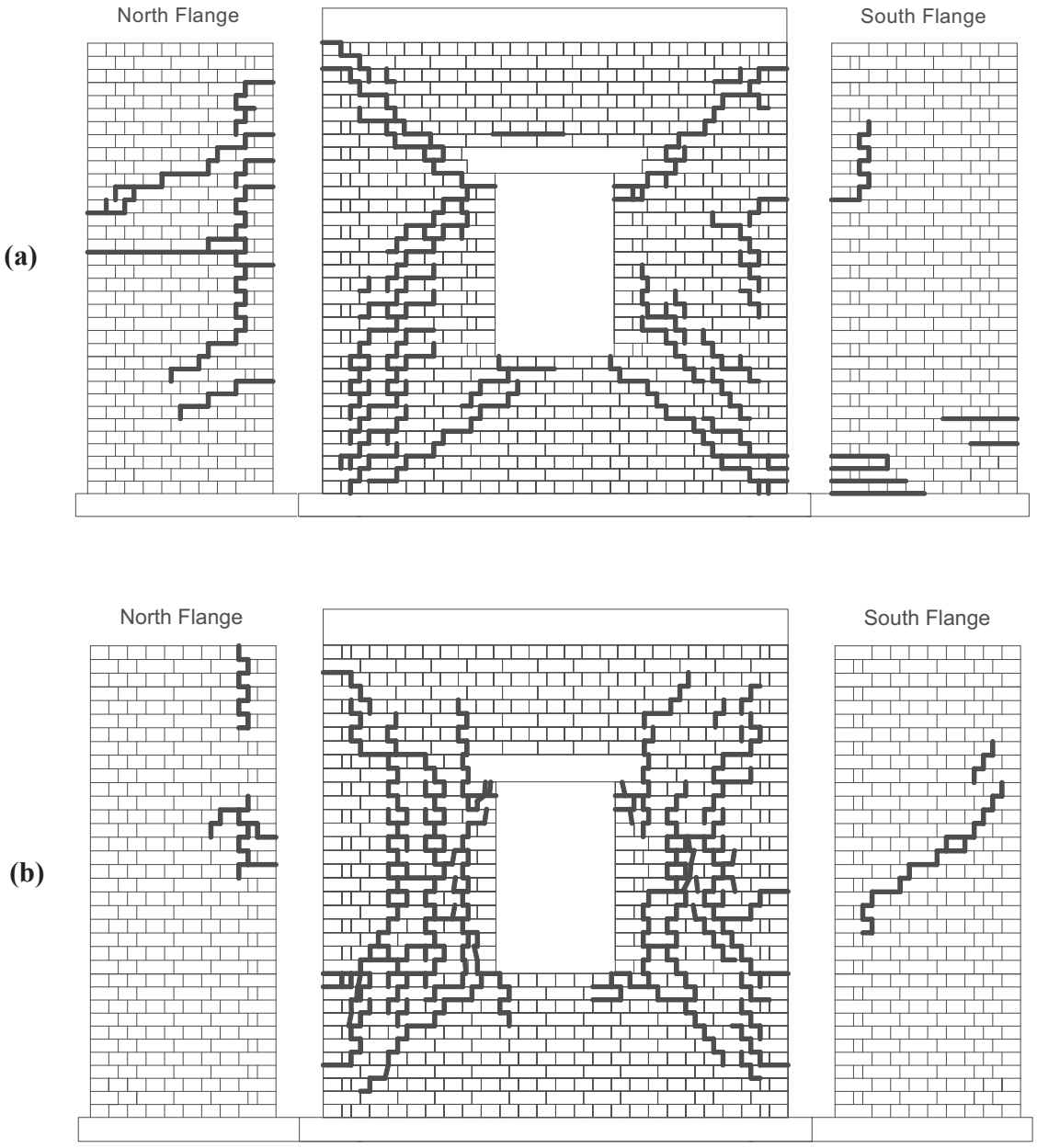

Fig. 12. Crack patterns: (a) SF1 wall, (b) SF2 wall.

and Beyer [42].

3.2.2. Wall S2

Very tight loops were observed till drift ratio of 0.18% as compared to 0.1% in previous specimens. This is also evident from damage mechanism that minimal damage was observed in the specimen till 0.18% drift ratio. Beyond this drift ratio cracks were observed at multiple locations in the specimens. Stiffness degradation started earlier in positive loading cycles. Contrary to specimen SF1, stiffness degraded more rapidly in positive cycles.

3.2.3. Wall SF1

Tight loops were observed till drift ratio of 0.1% indicating low energy dissipation. Stiffness degradation started during positive loading cycles first. However, stiffness degraded more rapidly during negative loading cycles as compared to positive loading cycles. Similar trend of strength degradation was observed in positive loading cycles till ultimate lateral resistance. Beyond ultimate resistance, strength degradation rate was similar in both negative and positive loading cycles.

3.2.4. Wall SF2

Less energy dissipation occurred till 0.18% drift ratio as evident from tight loops. Sudden loss in strength and stiffness occurred at 0.08% drift ratio due to the fact that multiple diagonal shear cracks appeared in the specimen at mid pier and lintel levels, as seen in Fig. 15. However, beyond this drift ratio till 0.18% drift ratio very less damage was observed and consequently strength and stiffness capacity continued to increase. Stiffness degradation started earlier in negative loading cycles and at more rapid rate as compared to positive loading cycles. This was a general trend observed in all test specimens except specimen SF1 where more control over target displacements might have yielded the same trend.

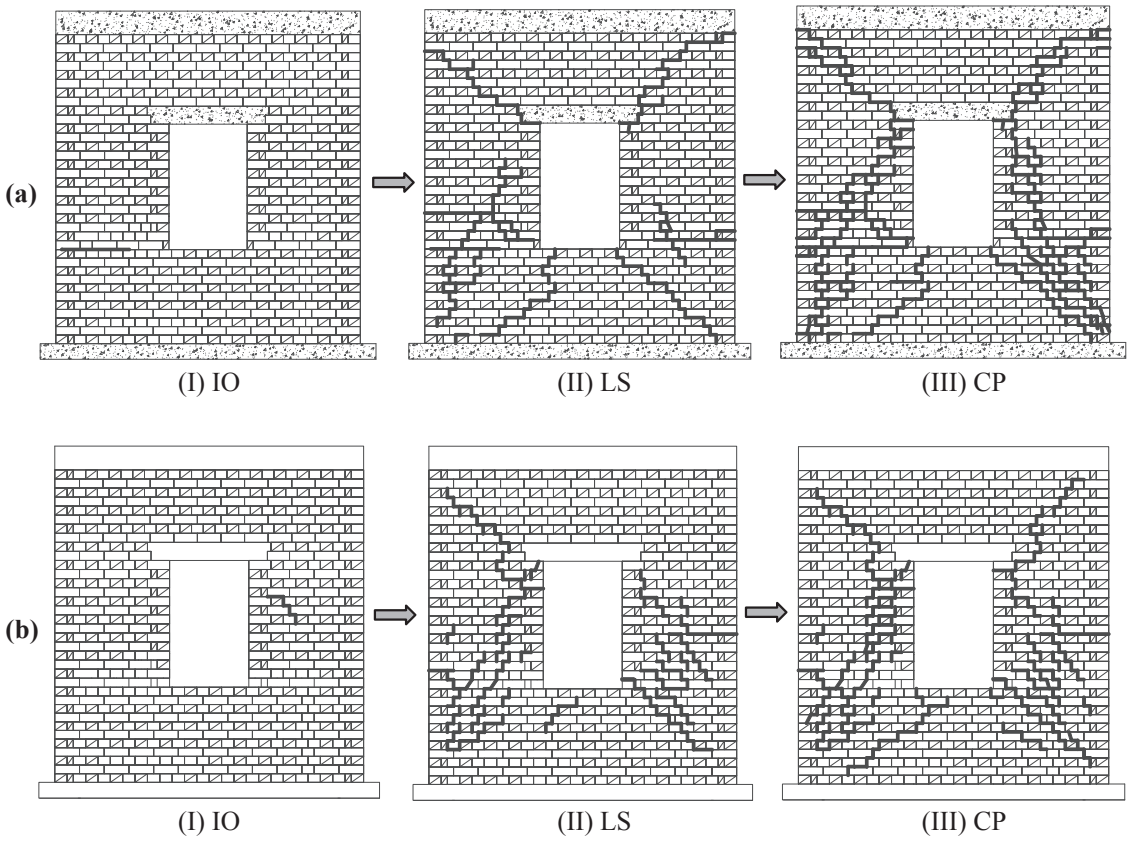

Fig. 13. Crack propagation at different limit states: (a) S1 wall, (b) S2 wall.

3.3. Energy dissipation mechanism

Damping curves of test specimens are presented in Fig. 18. Eq. (1) was used for determining equivalent viscous damping.

$$\xi_{eq} = \frac{E_d}{2\pi E_{inp}} \quad (1)$$

where E_d = dissipated energy (average of the areas of three displacement cycles at same displacement level) and E_{inp} = input energy (sum of half product of peak load and corresponding displacement in positive and negative loading cycles).

3.3.1. Wall S1

A mixed shear-flexural behavior can be observed from the damping curve of specimen S1 in Fig. 18. Average damping ratio of 20% was observed for specimen S1, as shown in Fig. 18. Maximum damping of 25% was observed at drift ratio of 0.20%. Beyond this drift ratio, the damping continued a decline trend indicating that no new cracks were observed in the specimen and rocking dominated the behavior for higher drift ratios. Study carried on masonry walls by Russell et al. [34] yielded almost similar energy dissipation. However, the studies carried out on masonry response by Javed [5], Ashraf [43,44] and Shahzada et al. [6] yielded significantly lower energy dissipation. The variation in energy dissipation can be attributed to the contribution of micro cracks in the specimen which led to high damping.

3.3.2. Wall S2

Average damping ratio of approximately 13.1% was observed in this specimen, as seen in Fig. 18. Shear behavior dominated energy dissipation. Damping continued an increasing trend in the later cycles due to appearance of new cracks.

3.3.3. Wall SF1

Average damping ratio of approximately 15.2% was observed in this specimen, as seen in Fig. 18. Due to initial diagonal shear cracks high energy dissipation occurred. From 0.08% to 0.17% drift ratio, very less number of cracks were observed and hence damping almost remain same, indicating a dominating flexure behavior during these drift ratios. Shear behavior was more dominated in this case. Beyond 0.17% drift ratio, shear behavior was more dominated and new shear cracks lead to increase in damping ratio.

3.3.4. Wall SF2

Average damping ratio of approximately 9.2% was observed in this specimen, as seen in Fig. 18. Shear behavior dominated energy dissipation in this case as well. Damping continued an increasing trend in the later cycles due to appearance of new cracks.

3.4. Bi-Linear idealization

Using equal energy principle, elasto-plastic bi-linear idealized curve was constructed for each specimen, as shown in Fig. 19. Using these idealized curves, elastic stiffness and displacement ductility factors were calculated for each specimen. Elastic stiffness (K_e) is the ratio of 0.75 V_u (where V_u = 0.9 V_{max}) to corresponding displacement. Displacement ductility (μ_D) is the ratio of ultimate displacement (Δ_u) to yield displacement (Δ_y). Δ_u corresponds to 0.8 V_u and $\Delta_y = V_u/K_e$. Table 3 present effective stiffness, displacement ductility factors, ultimate displacement and peak resistance for individual test specimens based on average loading values. Similarly, for SF1 specimen, effective stiffness was observed to be 38.71 kN/mm whereas for SF2 specimen an effective stiffness of 31.95 kN/mm was observed. For S1 specimen, effective stiffness of 37.68 kN/mm was observed whereas an effective stiffness of 29.75 kN/mm was observed for S2 specimen. As evident from the results, a very small increase was observed in effective stiffness

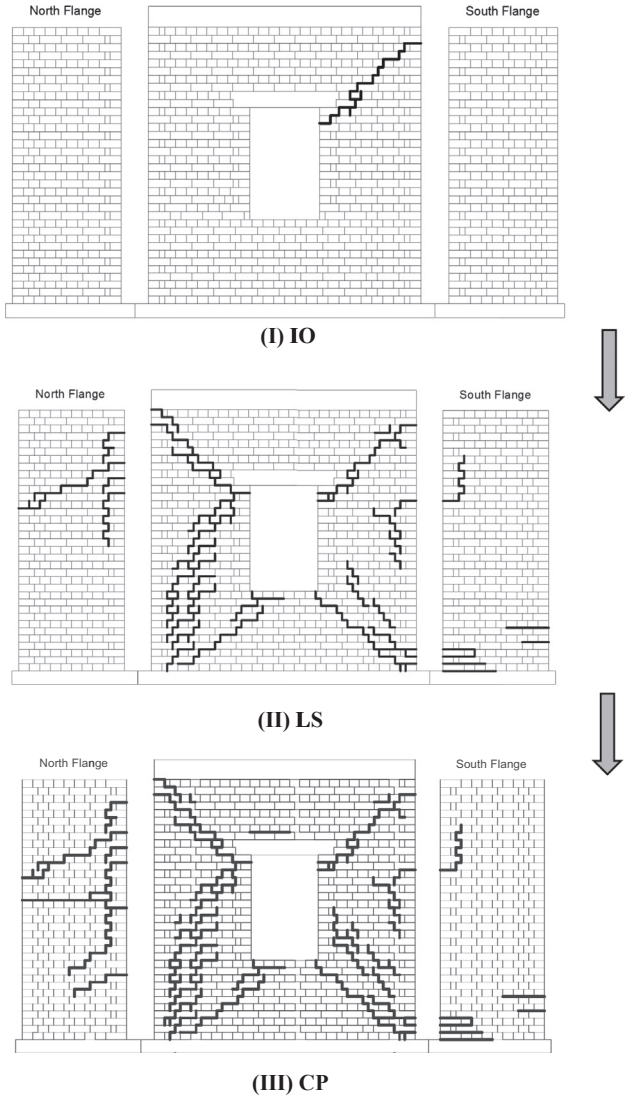

Fig. 14. Crack propagation at different limit states in specimen SF1.

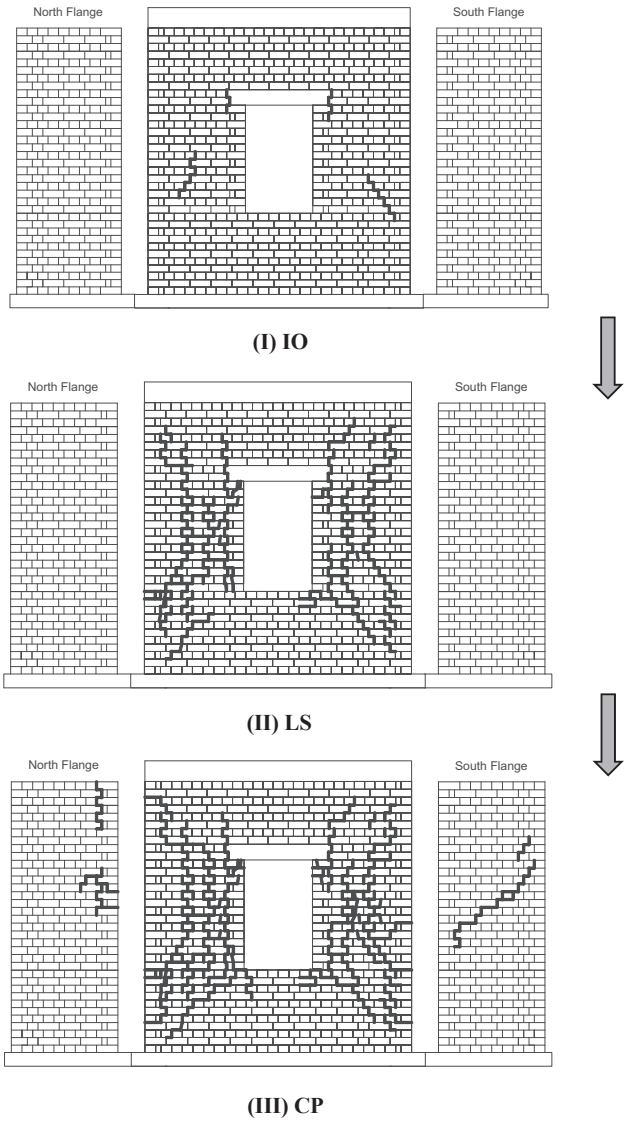

Fig. 15. Crack propagation at different limit states in specimen SF2.

of flanged specimens (SF1 and SF2). Displacement ductility for S1 and S2 specimens was calculated to be 13.07 and 6.20, respectively. This implies that increase in vertical stress resulted in 57% decrease in the displacement ductility of the specimens. For flanged specimens SF1 and SF2, the displacement ductility was calculated to be 15.43 and 7.20, respectively. These results suggest a similar decreasing trend in displacement ductility of flanged specimens after increasing vertical stresses. However, for both vertical stress levels, incorporation of flanges lead to increase in displacement ductility of specimens. For low vertical stress level, flanges increase the displacement ductility by 18%, whereas for high level of vertical stress an increase of 15% was observed in the displacement ductility of specimens. For both levels of vertical stresses, ultimate displacement increased after provision of flanges. For low vertical stress level, inclusion of flanges increase the ultimate displacement by 20%. For high vertical stress level, incorporation of flanges increase the ultimate displacement by 28%. These results highlight that increase in ultimate displacement is more prominent in case of high vertical stresses as compared to low vertical stresses. As shown in Table 3, peak resistance increased with increase in vertical stresses and provision of flanges. For S1 and S2, peak resistance was observed to be 27.26 kN and 68.24 kN, respectively. Hence increase in vertical stresses lead to an almost proportional increase in lateral resistance of specimen. For flanged specimens, SF1 and SF2, peak resistance was observed to be 31.43 kN and 75.70 kN, respectively. For both levels of vertical stresses, lateral resistance of masonry specimens increased. In case of low vertical stresses, an increase of 15% observed whereas an increase of 11% was observed for high level of vertical stresses. These values are based on average loading cycles of the test. However, the increasing trends remains the same for both positive and negative loading cycles amid slight variations.

Three performance levels; Immediate Occupancy (IO), Life Safety (LS) and Collapse Prevention (CP) are determined as per procedure described in ASCE/SEI 41-06 [40]. IO is the drift ratio that corresponds to yield displacement on the idealized elasto-plastic curve. At this point, no permanent deformation or strength degradation was observed in the specimen. CP is the ultimate drift ratio at which lateral strength degraded by 20% or test has stopped due to excessive deterioration of specimen. LS is taken as drift ratio that is 75% of CP. Table 4 represent building performance levels for each specimen. For IO performance level, storey drift of specimen S1 and SF1 almost remained same. However, for specimens subjected to high vertical stresses (S2 and SF2), a slight increase was observed in the storey drift values. For LS building performance level, specimen S1exhibited a storey drift of 0.22%. For same building performance level, specimen SF1 storey drift increase by almost 20% to a value of 0.27%. Similar increasing trend was observed for storey drifts corresponding to CP building performance level. An

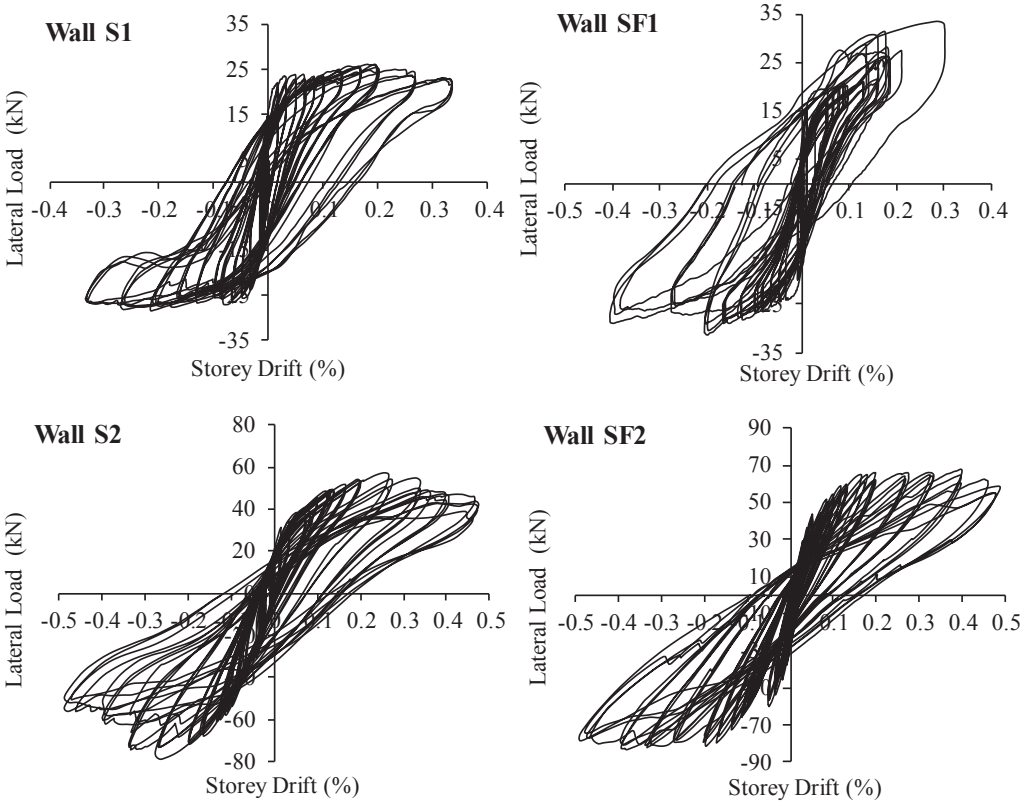

Fig. 16. Force-deformation hysteresis loops of test specimens.

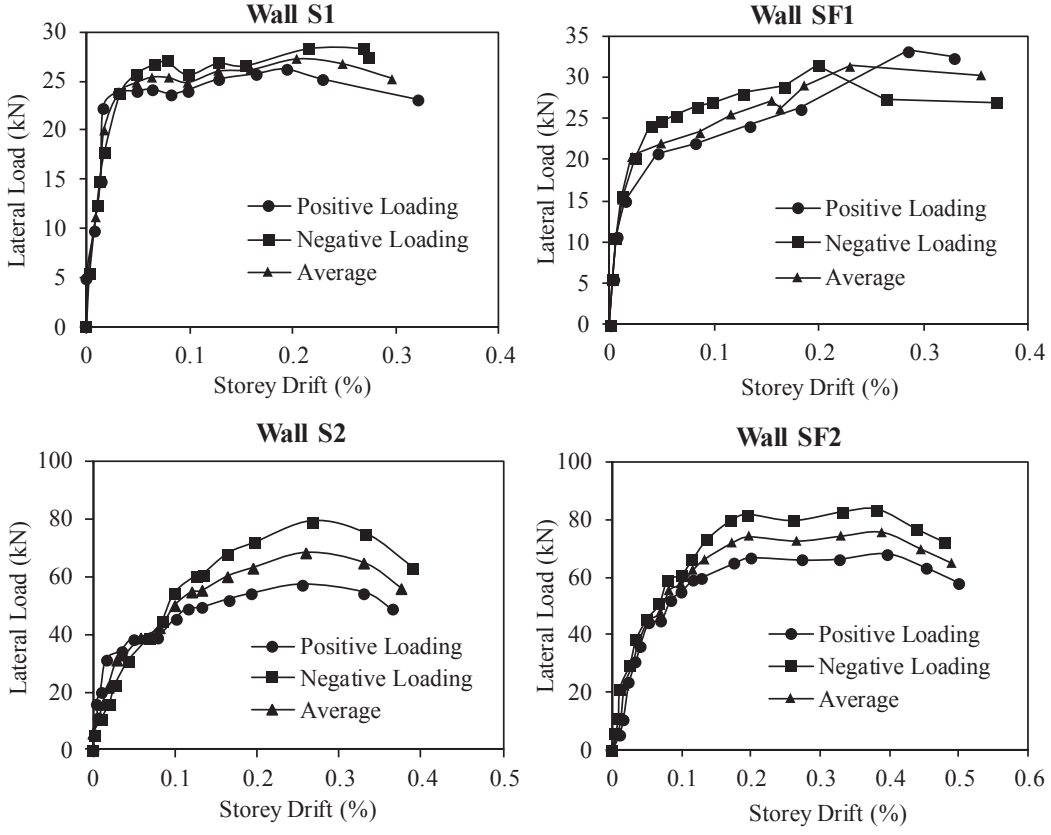

Fig. 17. Force-deformation envelope curves of test specimens.

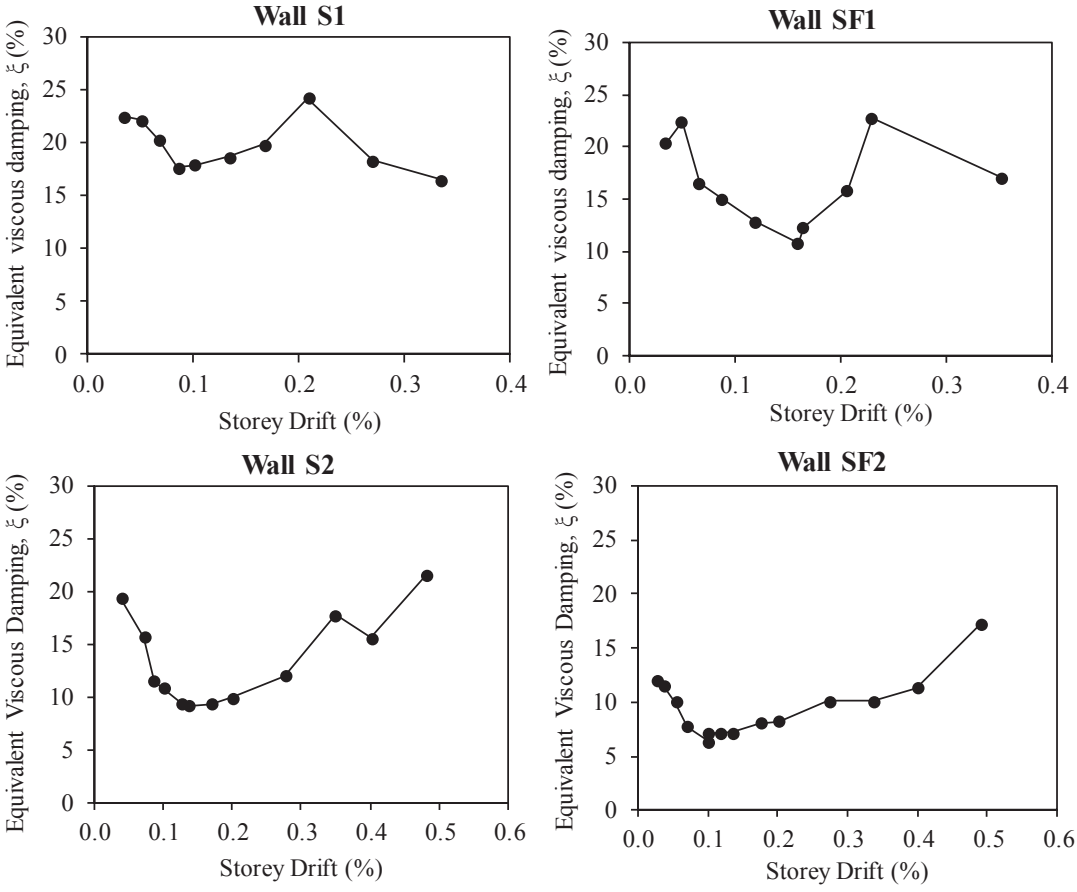

Fig. 18. Equivalent viscous damping of test specimens.

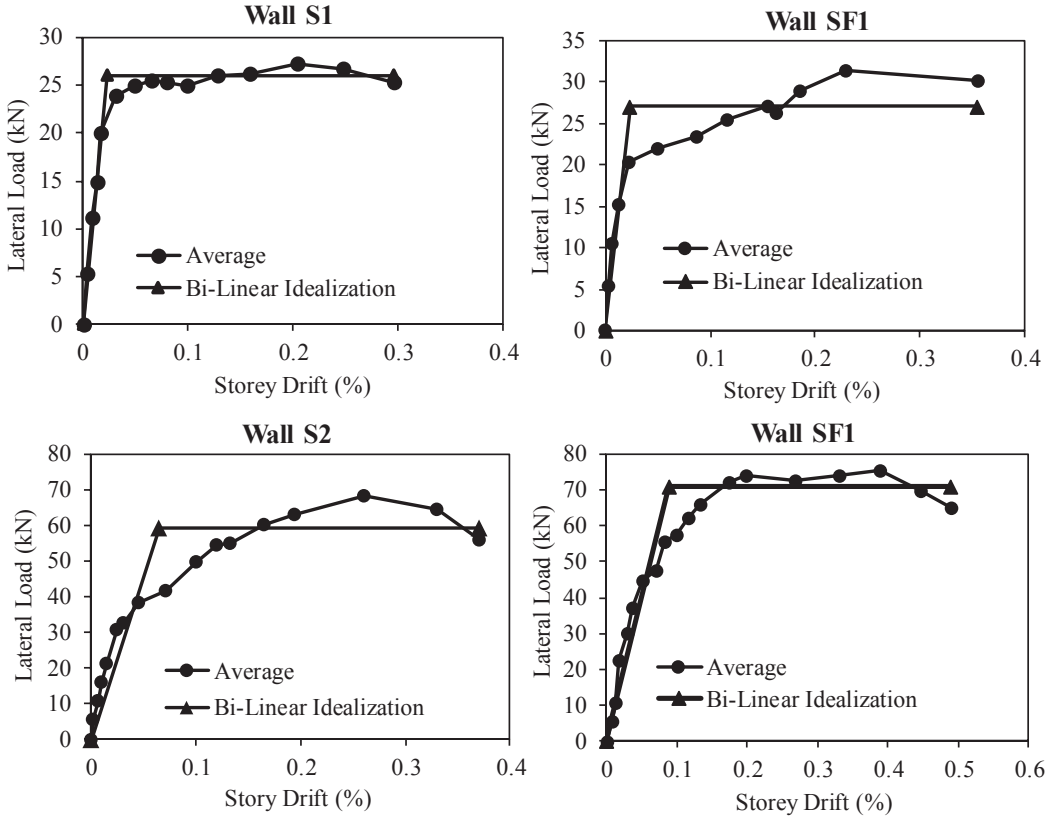

Fig. 19. Bi-Linear idealization of test specimens.

Table 3
Effective stiffness, displacement ductility, ultimate displacement and peak resistance of test specimens (Based on average loading values).

Specimen ID	Effective Stiffness, K_e (kN/mm)	Displacement Ductility, μ_D	Ultimate Displacement, Δ_u (mm)	Peak Resistance (kN)
S1	37.68	13.07	9.02	27.26
SF1	38.71	15.43	10.80	31.43
S2	29.75	6.70	12.39	68.24
SF2	31.95	7.20	15.85	75.70

Table 4
Building performance levels based on ASCE/SEI 41-06.

Specimen ID	Performance levels	Storey Drift (%)
S1	IO	0.05
	LS	0.22
	CP	0.30
SF1	IO	0.06
	LS	0.27
	CP	0.35
S2	IO	0.07
	LS	0.28
	CP	0.37
SF2	IO	0.08
	LS	0.39
	CP	0.52

increase of 33% in storey drift level corresponding to CP building performance was observed for flanged specimen subjected to high vertical stresses as compared to specimen without flanges with same vertical stress. It can therefore be concluded that provision of flanges increases the storey drift levels corresponding to different building performance levels. The increase in storey drift level was more prominent for LS and CP building performance levels.

3.5. Lateral strength

Lateral shear strength was measured herein to completely define the force-deformation behavior of specimens with and without flange incorporation. Lateral shear strength corresponding to different failure modes was evaluated for individual pier of each wall. Lateral strength was also evaluated based on the empirical models available in the literature. Due to the complexity of masonry material owing to its anisotropy and non-homogenous nature, accurate prediction of masonry strength becomes difficult. Empirical models recommended by ASCE 41-06 [40] and Magenes and Calvi 1997 [46] are commonly used in the literature to evaluate lateral shear strength capacity of unreinforced masonry corresponding to different failure modes. For flexural failure mode, which is characterized by rigid body motion and resulting bed joint cracks and toe crushing, the lateral shear resistance was estimated by using the following two equations as specified in ASCE 41-06 [40]:

$$V_{ro} = 0.9\alpha\left(\frac{pL_p^2 t_p}{H_p}\right) \tag{2}$$

$$V_{tc} = \alpha\left(\frac{pL_p^2 t_p}{H_p}\right)\left(1-\frac{p}{0.7f_m}\right) \tag{3}$$

where,

V_{ro} = lateral shear strength corresponding to rocking.
V_{tc} = lateral shear strength corresponding to toe crushing.
p = vertical stress on the pier.
L_p, H_p, t_p = length, height and thickness of pier.
α = boundary condition factor (for cantilever pier, α = 0.5, for fixed-fixed pier, α = 0.5).
f_m = compressive strength of masonry.

For diagonal tension failure mode, which is characterized by inclined and diagonal cracks that pass either through brick and mortar joint or brick units, the lateral shear resistance was calculated using the following equation, as discussed by Magenes and Calvi [46]:

$$V_{dt} = \frac{f_{tu} L_p t_p}{b}\sqrt{1+\frac{p}{f_m}} \tag{4}$$

where,

V_{dt} = lateral shear strength corresponding to diagonal tension.
f_{tu} = diagonal tensile strength of masonry.
b = shear stress distribution factor and can be expressed as $b = H_p/L_p$ ($1.0 \le b \le 1.5$).

Cracking lateral load, V_{cr}, of test specimens was calculated using the following equation:

$$V_{cr} = \frac{L_p^2 t_p}{6H_p}(p + f_{tu}) \tag{5}$$

For specimens subjected to low vertical stresses (S1 and SF1), lateral shear strength corresponding to rocking and toe crushing failure mode was estimated to be 34.20 kN and 36.95 kN, respectively. For these specimens lateral shear strength corresponding to diagonal tension failure mode was estimated to be 95.39 kN. However, maximum lateral strength of 28.36 kN and 33.31 kN was observed during negative cycles of the experiment for specimen S1 and SF1, respectively. These results comply with the fact that both S1 and SF1 exhibited dominant rocking mode of failure. For specimens subjected to high vertical stresses (S2 and SF2), lateral shear strength corresponding to rocking and toe crushing failure mode was estimated to be 92.96 kN and 95.64 kN, respectively. For these specimens, lateral shear strength corresponding to diagonal tension mode was estimate to be 119.20 kN. However, maximum lateral strength of 79.20 kN and 83.44 kN was observed during negative cycles of the experiment for specimen S2 and SF2, respectively. This corresponding to rocking/toe-crushing failure mode. However, the failure mode observed during the experiment was shear dominant. This difference in governing failure mode based on experimental results and empirical equations may be attributed to the cracking of brick units in the vicinity of toe. Cracking of these brick units before the initiation of diagonal cracks may have led to reduction in the diagonal shear capacity of the specimens. Such behavior was also reported by Ashraf 2010 [43].

Cracking lateral load was estimated for each specimen using Eq. (5). For specimens S1 and SF1, the cracking load was measured to be 6.42 kN. For these specimens, the cracking loads were observed to be 6.05 kN (S1) and 19.94 kN (SF1). For specimens S2 and SF2, cracking load was estimated to be 17.34 kN for these specimens the experimental cracking loads were observed to be 16.96 kN (S2) and 39.43 kN (SF2). Specimens with flanges exhibited much higher cracking load than those estimated using Eq. (5). However, for specimens without flanges, cracking load compare well with values estimated using Eq. (5).

3.6. Stiffness degradation

Stiffness degradation exhibited by test specimens during successive loading cycles was determined based on the average stiffness experienced by the specimens during positive and negative cycles. The average stiffness obtained was then normalized and plotted as a function of storey drift to analyze the stiffness degradation patterns during progressive loading cycles. The results are presented in Fig. 20. It can be observed that stiffness degraded at a rapid pace during initial phase of

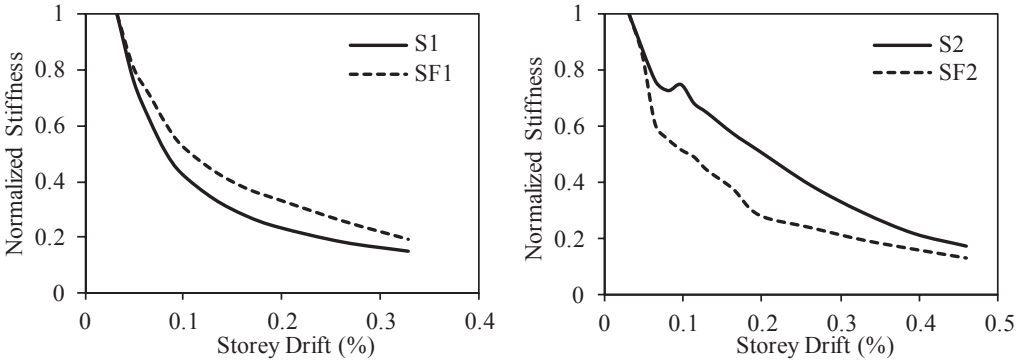

Fig. 20. Normalized stiffness degradation versus storey drift of test specimens.

testing. For specimens S1 and SF1, stiffness degradation occurred at a consistently rapid pace till 0.05% storey drift. Beyond this drift level, stiffness degradation continued at a relatively lower rate. This higher rate of stiffness degradation can be attributed to the initiation of cracks in the specimens. As evident from Fig. 20, stiffness degradation occurred more rapidly in specimen S1 and compared to specimen SF1. At 0.1% storey drift, specimen S1 experienced about 55% degradation in stiffness. For the same storey drift level, specimen SF1 experienced about 45% degradation in stiffness. Specimen S1 experienced 80% reduction in initial stiffness at storey drift level of 0.25%. Specimen SF1 experienced similar amount of degradation at 0.33% storey drift level. For specimens S2 and SF2, stiffness degradation occurred at a consistently rapid pace till 0.05% storey drift. Stiffness degradation occurred at a lower rate in both S2 and SF2 when compared with S1 and SF1 specimens. In contrast to stiffness degradation trend observed for Specimens S1 and SF1, the specimen SF2 experienced more stiffness degradation from its initial value as compared to specimen S2. During initial phase of loading, both specimen S2 and SF2 experienced stiffness degradation at same rate followed. Afterwards, stiffness degradation rate was more in case of specimen SF2. In later phase of loading, rate of stiffness degradation was relatively more in case of specimen S2 as compared to specimen SF2.

3.7. Global rocking

Global rocking of each test specimen was measured by installing displacement transducer for recording vertical displacement at the bottom of each specimen. The LVDT-6, as shown in Fig. 5 was used for recoding the global rocking behavior of each wall specimen. Vertical displacement data obtained from LVDT-6 is shown in Fig. 21. As evident from Fig. 21, specimen S1 exhibited negligible rocking till 0.15% drift ratio. Beyond 0.15% drift ratio, 0.8 mm rocking displacement was observed till 0.33% drift ratio. Relatively more rocking occurred in positive loading cycles as compared to negative loading cycles. In specimen S2, negligible rocking was observed in first few loading cycles. However, in later loading cycles, rocking was dominant and a maximum vertical displacement of 3.21 mm displacement was recorded in the last loading cycle. Contrary to specimen S1, relatively more rocking was recorded in negative loading cycles. Almost similar rocking behavior was observed in specimen SF2, as shown in Fig. 21. However, in contrast to specimen S2, specimen SF2 exhibited less rocking and a maximum vertical displacement of 2.82 mm was recorded. This

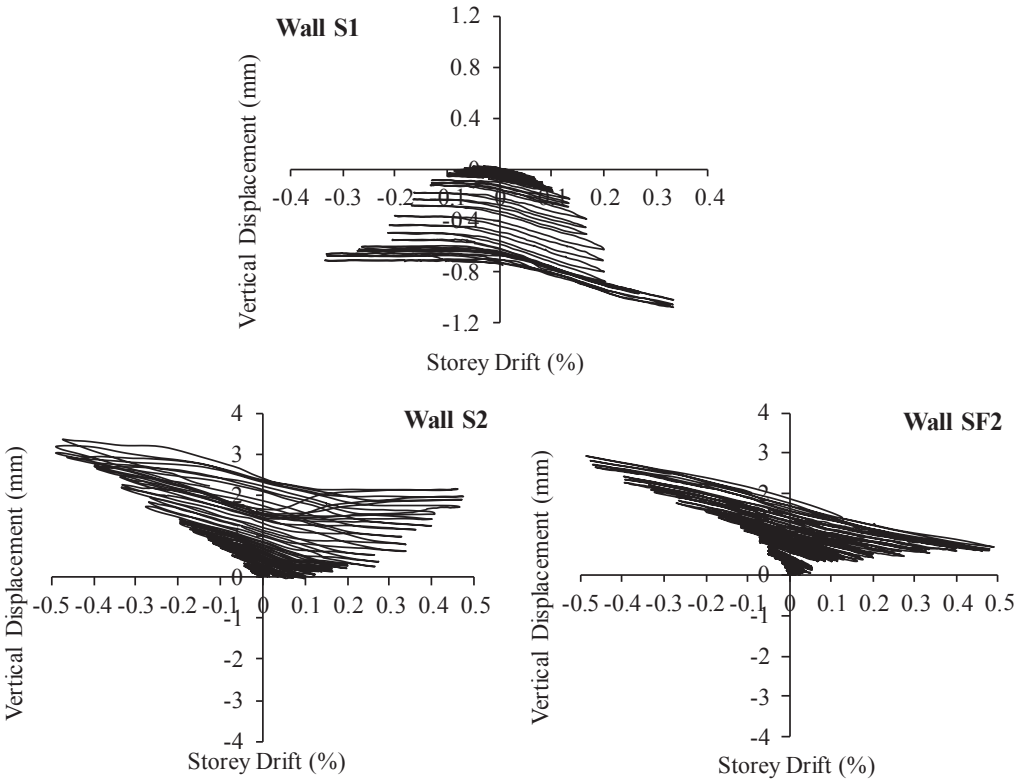

Fig. 21. Global rocking of test specimens.

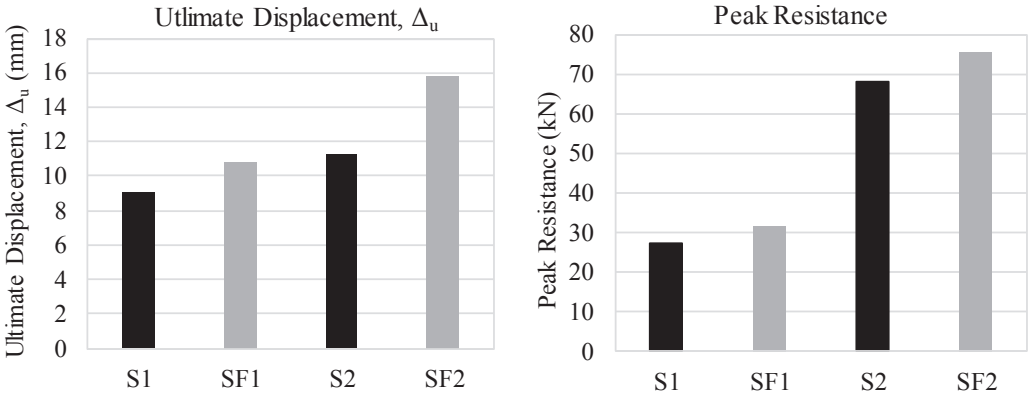

Fig. 22. Comparison of ultimate displacement and peak resistance of test specimens.

decrease in global rocking behavior of specimen SF2 compliment the damage mechanism exhibited by flanged specimens where incorporation of flanges shifted the flexure-dominated failure mode to shear-dominated failure mechanism.

3.8. Effects of flanges

In this section, the effects of flanges on various target parameters are discussed. To this end, effects of flanges on damage mechanism and force-deformation behavior of specimens were quantified. Damage mechanism was particularly affected by the inclusion of flanges. A small change from rocking to shear dominant mechanism was observed in case of flanged specimens (SF1 and SF2) which is in compliance with the results obtained by Moon et al. [29]. All specimens exhibited a dominant shear behavior followed by rocking. However, the extent of rocking was limited in case of specimens with flanges as compared to specimens without flanges (S1 and S2). This effect can be observed in the hysteretic loops of specimens in Fig. 16 and global rocking in Fig. 21. Same phenomena has been reported by Russell & Ingham [32].

Lateral strength of specimens increase by provisions of flanges (specimen SF1 and SF2), as evident from figure Fig. 22. Ultimate displacement of specimens increased for flanged specimens (SF1 and SF2). Both of these results are consistent with the results reported by (Yi et al. [31], Russell & Ingham [33] and Russell et al. [34].

Effective stiffness increased in case of flanged specimens (SF1 and SF2), as shown in Fig. 23. High increase in displacement ductility factor was observed for flanged specimens subjected to low vertical stresses whereas small increase was observed for flanged specimens subjected to high verticals stresses. High vertical stresses resulted in reduced displacement ductility factors.

4. Conclusions and recommendations

The objective of this study was to determine the effects of vertical stresses and flanges on the seismic behavior of URBM. Four full-scale perforated wall specimens were fabricated for studying the effects of above mentioned variables. Quasi-static testing was carried out on each test specimen and the data was analyzed to determine seismic behavior parameters that included force-deformation behavior, energy dissipation, stiffness and displacement ductility factors. A comparative study was then carried out to study the effects of vertical stresses and flanges on the strength and deformability characteristics of unreinforced masonry.

It is concluded that increase in vertical stresses in URBM results in dominating shear failure mode. Furthermore, increase in vertical stresses results in increasing the crack density thereby decreasing the crack width. For the same level of vertical stresses, provision of flanges in URBM tend to change the failure mode from rocking to shear. For low vertical stress case, the inclusion of flanges resulted in 18% increase in displacement ductility whereas ultimate displacement and peak resistance increased by 20% and 15%, respectively. A more prominent increasing trend is observed in case of high vertical stress conditions. For higher level of vertical stress, flanged specimen exhibited an increase of 15% in displacement ductility whereas ultimate displacement increased by 28%. Increase in vertical stress level improved the lateral resistance of flanged specimen by 11%. However, for high stress conditions, the increase in peak resistance capacity is lower than the former case. Stiffness degradation is observed to be affected by increasing the magnitude of vertical stresses and also by incorporation of flanges. Stiffness degradation rate is observed to be the same for both with and without flange specimens during earlier phase of loading. However, in case of high vertical stresses, stiffness degradation rate is decreased in higher loading cycles for flanged specimen. Furthermore, equivalent viscous damping decreased in both vertical stress conditions after

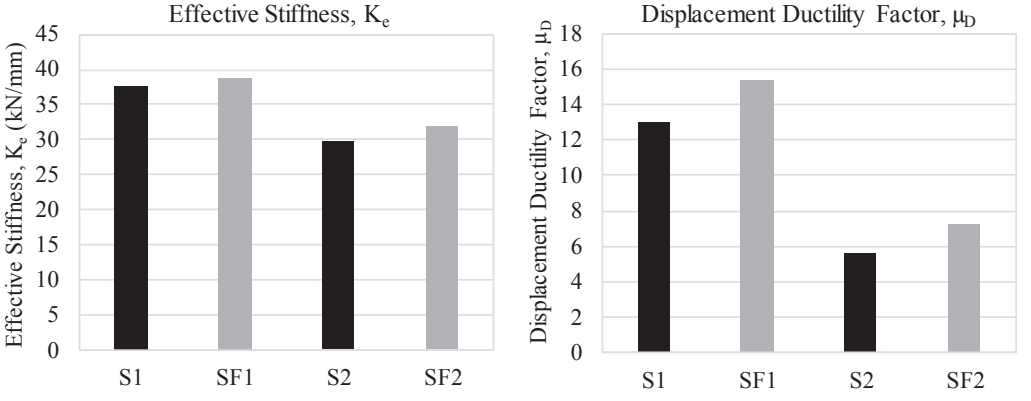

Fig. 23. Comparison of effective stiffness and displacement ductility factors of test specimens.

inclusion of flanges.

The scope of this study is limited to vertical stresses resulting from single and double storey loads experienced in typical URBM in Pakistan. Future studies need to include a broad range of vertical stresses and provision of flanges on different sides of in-plane walls to further explore the sensitivity of seismic parameter for higher vertical stresses and flanges.

Acknowledgement

The authors are thankful to the Board of Advance Studies and Research (BOASAR) University of Engineering and Technology, Peshawar, Pakistan for partial funding for this project.

References

[1] Tomazevic M. Earthquake-Resistant Design of Masonry Buildings. First Ed. Singapore: Imperial College Press, London; 1999.
[2] Durrani AJ, Elnashai AS, Hashash Y, Kim SJ, Masud A. The Kashmir Earthquake of October 8, 2005: A Quick Look Report. USA: Mid-America Earthquake Center, University of Illonoi at UC; 2005. http://hdl.handle.net/2142/8937.
[3] Javed M, Khan AN, Penna A, Magenes G. Behavior of Masonry Structures During the Kashmir 2005 Earthquake. Proceedings of First European Confer-ence on Earthquake Engineering and Seismology Geneva, Switzerland. Paper No. 1077. 2006.
[4] Ali, Q. Unreinforced Brick Masonry Residential Building.*EERI World Housing Encyclopedia,* 2006 Report No. 159.
[5] Javed M. Seismic Risk Assessment of Unreinforced Brick Masonry Buildings System of Northern Pakistan. Ph. D. Dissertation. University of Engineering and Technology, Peshawar, Pakistan. Link: eprints.hec.gov.pk. 2009.
[6] Shahzada K, Khan AN, Elnashai AS, Ashraf M, Javed M, Naseer A, et al. Experimental seismic performance evaluation of unreinforced brick masonry buildings. Earthquake Spectra 2012;28(3):1269–90. http://dx.doi.org/10.1193/1.4000073.
[7] Ahmad N. A Note on The Strong Ground Motions and Behavior of Buildings During 26th Oct. 2015 Afghanistan-Pakistan Earthquake. Earthquake Engineering Center, University of Engineering and Technology Peshawar, Pakistan. 2015 (EERI Report).
[8] Ismail N, Khattak N. Reconnaissance report on the Mw 7.5 Hindu Kush earthquake of 26th October 2015 and the subsequent aftershocks. Department of Civil and Environmental Engineering, Faculty of Engineering, United Arab Emirates University. 2015 (EERI Report).
[9] Çelebi M, Bazzurro P, Chiaraluce L, Clemente P, Decanini L, DeSortis A, et al. Recorded motions of the 6 April 2009 Mw 6.3 L'Aquila, Italy, earthquake and implications for building structural damage: overview. Earthquake Spectra 2010;26(3):651–84. http://dx.doi.org/10.1193/1.3450317.
[10] Braga F, Manfredi V, Masi A, Salvatori A, Vona M. Performance of non-structural elements in RC buildings during the L'Aquila, 2009 Earthquake. Bull Earthq Eng 2011;9(1):307–24. http://dx.doi.org/10.1007/s10518-010-9205-7.
[11] Geotechnical Extreme Events Reconnaissance (GEER). 2017. Engineering Reconnaissance following the October 2016 Central Italy Earthquakes. Report No. GEER-050C.
[12] Cimellaro GP. Field reconnaissance on August 25th, after August 24th, 2016 Central Italy Earthquake. Pacific Engineering Research Center (PEER) Presentation. 2016.
[13] Dizhur Dmytro, Dhakal Rajesh P, Bothara Jitendra, Ingham Jason M. Building typologies and failure modes observed in the 2015 Gorkha (Nepal) earthquake. Bulletin New Zealand Soc Earthquake Eng 2016;49(2):211–32http://hdl.handle.net/2292/29076.
[14] Gautam Dipendra, Chaulagain Hemchandra. Structural performance and associated lessons to be learned from world earthquakes in Nepal after 25 April 2015 (M W 7.8) Gorkha earthquake. Eng Fail Anal 2016;68:222–43. http://dx.doi.org/10.1016/j.engfailanal.2016.06.002.
[15] Magenes G, Calvi GM. Shaking Table Tests on Brick Masonry Walls. The 10th Europ Conf Earthquake Eng. Vienna: Austria; 1994. p. 2419–24.
[16] Irimies M, Bia C. Cyclic Loading Behavior of A Perforated Unreinforced Masonry Wall Model. Proceedings of 12th World Conference on Earthquake Engineering. New Zealand. 2000.
[17] Yi W, Oh S, Lee J. Shear Capacity Assessment of Unreinforced Masonry Wall. 13th World Conference on Earthquake Engineering, 2004 (1698) 1–12.
[18] Haach VG, Vasconcelos G, Lourenço PB. Parametrical study of masonry walls subjected to in-plane loading through numerical modeling. Eng Struct 2011;33(4):1377–89. http://dx.doi.org/10.1016/j.engstruct.2011.01.015.
[19] Tomaževič M, Weiss P. Robustness as a criterion for use of hollow clay masonry units in seismic zones: an attempt to propose the measure. Mater Struct 2012;45(4):541–59. http://dx.doi.org/10.1617/s11527-011-9781-2.
[20] Salmanpour A, Mojsilovic N, Schwartz J. Experimental Study of the Deformation Capacity of Structural Masonry. In Proceedings, 12th Canadian Masonry Symposium, Vancouver 2012, British Columbia, June 2–5, 2013, Paper No. 161.
[21] Salmanpour AH, Mojsilovic N, Schwartz J. Deformation capacity of unreinforced masonry walls subjected to in-plane loading: a state-of-the-art review. Internat J Adv Struct Eng 2013;5(1):22. http://dx.doi.org/10.1186/2008-6695-5-22.
[22] Salmanpour AH, Mojsilović N, Schwartz J. Displacement capacity of contemporary unreinforced masonry walls: an experimental study. Eng Struct 2015;89:1–16. http://dx.doi.org/10.1016/j.engstruct.2015.01.052.
[23] Javed M, Magenes G, Alam B, Khan AN, Ali Q, Syed AM. Experimental seismic performance evaluation of unreinforced brick masonry shear walls. Earthquake Spectra 2015;31(1):215–46. http://dx.doi.org/10.1193/111512EQS329M.
[24] Calvi MG, Kingsley GR, Magenes G. Testing of masonry structures for seismic assessment. Earthq. Spectra 1996;12(1):145–62. http://dx.doi.org/10.1193/1.1585872.
[25] Tomaževič M, Lutman M, Weiss P. The seismic resistance of historical urban buildings and the interventions in their floor systems: an experimental study. The Masonry Soc J 1993:77–86.
[26] Costley AC, Abrams DP. Dynamic Response of Unreinforced Masonry Buildings with Flexible Diaphragms. NCEER-96-0001, University of Buffalo, Buffalo, N.Y., USA 1996.
[27] Paquette J, Bruneau M. Pseudo-dynamic testing of unreinforced masonry building with flexible diaphragm. J Struct Eng 2003;129(6):708–16. http://dx.doi.org/10.1061/(ASCE)0733-9445(2003) 129:6(708).
[28] Moon FL. Seismic Strengthening of Low-Rise Unreinforced Masonry Structures With Flexible Diaphragms. PhD Thesis, (May). 2004 http://hdl.handle.net/1853/5128.
[29] Yi T, Moon FL, Leon RT, Kahn LF. Analyses of a two-story unreinforced masonry building. J Struct Eng 2006;132(5):653–62. http://dx.doi.org/10.1061/(ASCE)0733-9445(2006) 132:5(653).
[30] FEMA. 2000. Prestandard and Commentary for the Seismic Rehabilitation of Buildings. FEMA 356, Washington, DC.
[31] Yi T, Moon FL, Leon RT, Kahn LF. Flange effects on the non-linear behavior of URM Piers. Masonry Soc J 2008;26(2):31–42.
[32] Russell AP, Ingham JM. Flange Effects of an Unreinforced Masonry Wall Subjected to Pseudo-Static In-Plane Seismic Forces. In The 14th World Conference on Earthquake Engineering. Beijing. 2008 http://hdl.handle.net/2292/25979.
[33] Russell AP, Ingham JM. The Influence of Flanges on the In-Plane Seismic Performance of URM Walls in New Zealand Buildings. In New Zealand Society of Earthquake Engineering Conference. 2010 Paper No. 38.
[34] Russell AP, Elwood KJ, Ingham JM. Lateral force-displacement response of unreinforced masonry walls with flanges. J Struct Eng 2014;140(4). http://dx.doi.org/10.1061/(ASCE)ST.1943-541X.0000863.
[35] Khanmohammadi M, Behnam H, Marefat MS. Seismic behavior prediction of flanged unreinforced masonry (FURM) walls. J Earthquake Eng 2014;18(5):759–84. http://dx.doi.org/10.1080/13632469.2014.897273.
[36] ASTM International.*ASTM C67-16 Standard Test Methods for Sampling and Testing Brick and Structural Clay Tile*. West Conshohocken, PA: ASTM International, 2016. doi: https://doi.org/10.1520/C0067-16.
[37] ASTM International. 2016. ASTM C109/C109M-16a Standard Test Method for Compressive Strength of Hydraulic Cement Mortars (Using 2-in. or [50-mm] Cube Specimens). West Conshohocken, PA: ASTM International. doi: 10.1520/C0109_C0109M-16A.
[38] ASTM International. ASTM C1314–16 Standard Test Method for Compressive Strength of Masonry Prisms. West Conshohocken, PA: ASTM International; 2016. http://dx.doi.org/10.1520/C1314-16.
[39] ASTM International. ASTM E519/E519M-15 Standard Test Method for Diagonal Tension (Shear) in Masonry Assemblages. West Conshohocken, PA: ASTM International; 2015. http://dx.doi.org/10.1520/E0519_E0519M-15.
[40] ASCE/SEI. 2007. Seismic Rehabilitation of Existing Buildings. ASCE/SEI 41–06, Reston, VA, USA.
[41] Petry S, Beyer K. Influence of boundary conditions and size effect on the drift capacity of URM walls. Eng Struct 2014;65:76–88. http://dx.doi.org/10.1016/j.engstruct.2014.01.048.
[42] Petry S, Beyer K. Limit states of modern unreinforced clay brick masonry walls subjected to in-plane loading. Bull Earthq Eng 2015;13(4):1073–95. http://dx.doi.org/10.1007/s10518-014-9695-9.
[43] Ashraf, M. 2010. Development of Low-cost and Efficient Retrofitting Technique for Unreinforced Masonry Buildings. PhD Dissertation, *University of Engineering and Technology, Peshawar, Pakistan.* Link: http://eprints.hec.gov.pk/9628/.
[44] Ashraf M, Khan AN, Naseer A, Ali Q, Alam B. Seismic behavior of unreinforced and confined brick masonry walls before and after ferrocement overlay retrofitting. Internat J Architect Heritage 2012;6(6):665–88.
[45] Petry S, Beyer K. Scaling unreinforced masonry for reduced-scale seismic testing. Bull Earthq Eng 2014;12(6):2557–81.
[46] Magenes G, Calvi GM. In-plane seismic response of brick masonry walls. Earthquake Eng Struct Dynam 1997;26:1091–112.